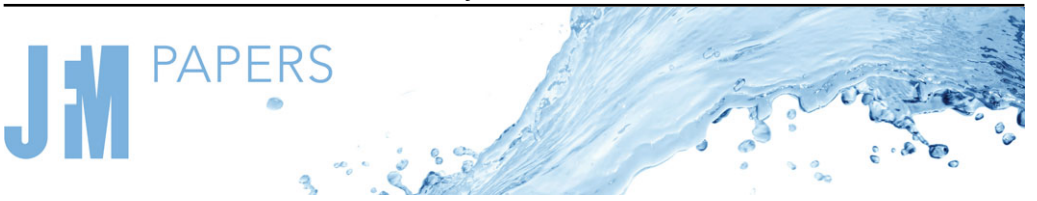
J. Fluid Mech. (2025), *vol.* 1012, A28, doi:10.1017/jfm.2025.10214



A nonlinear Schrödinger equation for capillary waves on arbitrary depth with constant vorticity

Christian Kharif[1], **Malek Abid**[1], **Yang-Yih Chen**[2] and **Hung-Chu Hsu**[2]

[1]Aix-Marseille Université, Institut de Recherche sur les Phénomènes Hors Equilibre, UMR 7342, CNRS, Centrale Méditerranée, Marseille 13384, France

[2]Department of Marine Environment and Engineering, National Sun Yat-Sen University, Kaohsiung 80424, Taiwan

Corresponding author: Christian Kharif, kharif@irphe.univ-mrs.fr

(Received 6 April 2024; revised 19 December 2024; accepted 1 May 2025)

A nonlinear Schrödinger equation for pure capillary waves propagating at the free surface of a vertically sheared current has been used to study the stability and bifurcation of capillary Stokes waves on arbitrary depth. A linear stability analysis of weakly nonlinear capillary Stokes waves on arbitrary depth has shown that (i) the growth rate of modulational instability increases as the vorticity decreases whatever the dispersive parameter kh, where k is the carrier wavenumber and h the depth; (ii) the growth rate is significantly amplified for shallow water depths; and (iii) the instability bandwidth widens as the vorticity decreases. Particular attention has been paid to damping due to viscosity and forcing effects on modulational instability. In addition, a linear stability analysis to transverse perturbations in deep water has been carried out, demonstrating that the dominant modulational instability is two-dimensional whatever the vorticity. Near the minimum of linear phase velocity in deep water, we have shown that generalised capillary solitary waves bifurcate from linear capillary Stokes waves when the vorticity is positive. Moreover, we have shown that the envelope of pure capillary waves in deep water is unstable to transverse perturbations. Consequently, deep-water generalised capillary solitary waves are expected to be unstable to transverse perturbations.

Key words: bifurcation, capillary waves, shear-flow instability

1. Introduction

The effect of wind blowing above the air–sea interface is twofold: (i) it generates short waves that take place within the first millimetres to metres and (ii) it generates a shear flow in the uppermost layer of the water. Consequently, these waves propagate in the

© The Author(s), 2025. Published by Cambridge University Press.

https://doi.org/10.1017/jfm.2025.10214 Published online by Cambridge University Press

presence of vorticity. These small scales participate in the exchanges of momentum, energy and mass across the air–sea interface. An accurate description of the surface stress is important in modelling and forecasting ocean wave dynamics. In addition, knowledge of their properties is crucial for satellite remote sensing applications.

In this paper, we focus our study on weakly nonlinear capillary waves propagating at the free surface of a flow of constant vorticity. One of our aims is to complete and extend to finite depth the preliminary results of Hsu *et al.* (2018) and Dhar & Kirby (2023) on pure capillary waves on deep water in the presence of constant vorticity. Hsu *et al.* (2018) used a cubic nonlinear Schrödinger (NLS) equation, whereas Dhar & Kirby (2023) used a fourth-order NLS equation. Hsu *et al.* (2018) investigated the effect of a shear current of constant vorticity on the modulational instability of weakly nonlinear periodic gravity–capillary wave trains. To do this, they derived a cubic NLS equation for gravity–capillary water waves on arbitrary depth with constant vorticity. To extend their results in the absence of acceleration due to gravity, we consider the NLS equation for pure capillary water waves on finite-depth currents of constant vorticity. Later on, within the framework a fourth-order NLS equation Dhar & Kirby (2023) investigated the stability of periodic gravity–capillary waves on arbitrary depth in the presence of constant vorticity. To the best of our knowledge, there is no study on the stability of pure capillary waves on finite depth in the presence of constant vorticity.

On the other hand, several studies have been devoted to the stability of steadily propagating periodic capillary waves on deep water, but without vorticity. Chen & Saffman (1985) investigated the three-dimensional stability and bifurcation of capillary waves and gravity waves on deep water. To do this, they used the approach detailed by McLean (1982*b*) for fully nonlinear waves and the NLS equation for the modulational instability of weakly nonlinear capillary waves. Hogan (1985) derived from the Zakharov equation a fourth-order NLS equation in deep water and found that the mean flow effect on weakly nonlinear pure capillary waves is of opposite sign to that on pure gravity waves. Zhang & Melville (1986) considered the stability of weakly nonlinear gravity–capillary waves on deep water in the range of capillary waves of a few millimetres. They focused their study on triad and quartet instabilities. Hogan (1988) found two superharmonic bubbles of instability of the exact nonlinear capillary wave solutions of Crapper (1957) at amplitudes less than the maximum. Tiron & Choi (2012) investigated the stability of the exact deep-water capillary waves (Crapper's solutions). They found that Crapper's capillary waves are stable to superharmonic disturbances whatever the amplitude and unstable to subharmonic disturbances. Later on, Murashige & Choi (2020) considered the stability of Crapper's capillary waves on deep water to weakly three-dimensional disturbances. They found that Crapper's solutions are stable to two-dimensional superharmonic disturbances and unstable to three-dimensional superharmonic disturbances.

In the absence of vorticity, the existence of solitary gravity–capillary waves on deep water was proved numerically by Longuet-Higgins (1989). Later on, Akylas (1993), using the NLS equation in deep water, showed that gravity–capillary solitary waves occur when the phase velocity of the carrier wave matches the group velocity of the envelope soliton solution. The linear dispersion relation of gravity–capillary waves has a minimum in phase velocity, which is equal to the group velocity. Consequently, for values less than this extremum, two-dimensional gravity–capillary waves may bifurcate into solitary waves in deep water. Abid *et al.* (2019) found that gravity–capillary solitary waves with decaying oscillatory tails exist in deep water in the presence of constant vorticity. For a review on this problem, one can refer to Dias & Kharif (1999). Steady three-dimensional gravity–capillary waves were investigated by Kim & Akylas (2005), Milewski (2005) and Părău *et al.* (2005). To the best of our knowledge, this bifurcation phenomenon has

https://doi.org/10.1017/jfm.2025.10214 Published online by Cambridge University Press

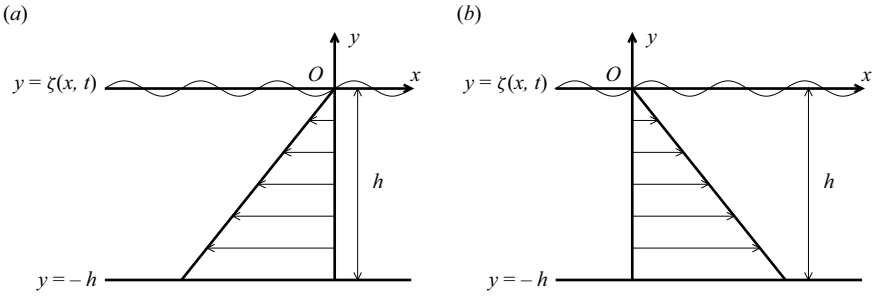


Figure 1. Sketches of waves on a shear current in the moving reference frame. Downstream propagation (*a*). Upstream propagation (*b*).

not been considered for pure capillary waves. This can be easily understood, since the linear dispersion relation of pure capillary waves has no minimum in phase velocity in the absence of vorticity.

In § 2 the NLS equation for capillary waves is given, and the physical phenomena associated with the singularities of the nonlinear coefficient are discussed. Section 3 is devoted to the stability analysis of periodic capillary waves on arbitrary depth in the presence of constant vorticity. Bifurcation of generalised solitary waves on deep water from periodic capillary wave trains is considered in § 4. Transverse instability of capillary envelope soliton and uniform capillary wave trains in deep water is considered in § 5.

2. Nonlinear Schrödinger equation for pure capillary waves

The unperturbed flow is a weakly nonlinear capillary wave train travelling steadily at the free surface of a vertically sheared current of constant vorticity (see figure 1). The fluid is assumed incompressible and inviscid.

In the fixed frame, the underlying current velocity is $u_0(y) = U_0 + \Omega y$, where Ω is the shear (the current intensity) and U_0 the current velocity at the free surface $y = 0$. The waves are stationary on a stream. Note that the vorticity is $-\Omega$. Downstream propagation corresponds to negative vorticity, whereas upstream propagation corresponds to positive vorticity.

Being primarily interested in the effect of the vorticity, we choose a reference frame moving with U_0 (see figure 1). In the moving frame, the fluid velocity is

$$\mathbf{u}(x, y) = (\Omega y + \phi_x, \phi_y), \tag{2.1}$$

where (ϕ_x, ϕ_y) is the wave-induced velocity.

The waves are potential due to the Kelvin theorem, which states that vorticity is conserved for a two-dimensional flow of an incompressible and inviscid fluid with external forces derived from a potential. There is no loss of generality if the study is restricted to carrier waves with positive phase speeds, so long as both positive and negative values of Ω are considered.

The governing equations are the Laplace equation (2.2) with the kinematic and dynamic boundary conditions (2.3)–(2.4) and the bottom condition (2.5):

$$\Delta\phi(x, y, t) = 0, \quad -h < y < \zeta(x, t), \tag{2.2}$$

where $\zeta(x, t)$ is the surface elevation,

$$\zeta_t + \zeta_x(\phi_x + \Omega y) - \phi_y = 0, \quad y = \zeta(x, t), \tag{2.3}$$

$$\phi_t + \frac{1}{2}(\nabla\phi)^2 + \Omega\zeta\phi_x - \Omega\psi - \frac{T}{\rho_w}\frac{\zeta_{xx}}{(1+\zeta_x^2)^{3/2}} = -\frac{P_a}{\rho_w}, \quad y = \zeta(x, t), \tag{2.4}$$

https://doi.org/10.1017/jfm.2025.10214 Published online by Cambridge University Press

where ψ is the stream function and ρ_w the water density. The surface tension T is assumed constant.

Without loss of generality, the atmospheric pressure, P_a, is set equal to zero:

$$\phi_y = 0, \quad y = -h. \tag{2.5}$$

Following Thomas, Kharif & Manna (2012) and Hsu *et al.* (2018), the stream function ψ can be removed by differentiating (2.4) with respect to x and using the Cauchy–Riemann relations. (Here $f(z) = \phi(x, y) + i\psi(x, y)$ with $z = x + iy$ where ϕ is harmonic and $\psi = H(\phi)$ its Hilbert transform. Consequently, f is holomorphic and satisfies the Cauchy–Riemann relations.) The dynamic boundary condition becomes for weakly nonlinear water waves

$$\begin{aligned}&\phi_{tx} + \phi_{ty}\zeta_x + \phi_x(\phi_{xx} + \phi_{xy}\zeta_x) + \phi_y(\phi_{xy} + \phi_{yy}\zeta_x) + \Omega\zeta(\phi_{xx} + \phi_{xy}\zeta_x) + \Omega\phi_y \\ &\quad - \frac{T}{\rho_w}\left(\zeta_{xxx} - \frac{3}{2}\zeta_x^2\zeta_{xxx} - 3\zeta_{xx}^2\zeta_x\right) = 0, \quad y = \zeta(x, t).\end{aligned} \tag{2.6}$$

Equation (2.6) corresponds to that of Hsu *et al.* (2018) for $g = 0$.

Hsu *et al.* (2018) used the method of multiple scales to derive the spatio-temporal evolution of the complex envelope, $a(\xi, \tau)$, of the free surface elevation $\zeta(x, t)$:

$$\zeta(x, t) = \frac{1}{2}\{\epsilon a(\xi, \tau)\exp(i(kx - \omega t)) + \text{c.c.}\} + \mathcal{O}(\epsilon^2), \tag{2.7}$$

where $\xi = \epsilon(x - c_g t)$, $\tau = \epsilon^2 t$, c_g, k and ω are the group velocity, wavenumber and frequency of the carrier wave and ϵ a small parameter.

2.1. *Expression of dispersive and nonlinear coefficients*

To obtain the dispersive and nonlinear coefficients L and N of the vor-NLS equation for pure capillary wave trains, we used the expressions we derived for gravity–capillary waves in finite depth and in the presence of vorticity (see equation (2.31) of Hsu *et al.* (2018)) when κ goes to infinity. The limit of the dispersive coefficient is obtained easily whereas the limit of the nonlinear coefficient needs to be handled carefully because two terms go to infinity. Fortunately, these two infinite terms cancel each other as is shown in the Appendix.

The NLS equation governing the evolution of the complex envelope of a packet of capillary waves on finite depth in the presence of constant vorticity (vor-NLS) is

$$ia_\tau + La_{\xi\xi} + N|a|^2 a = 0, \tag{2.8}$$

with

$$\begin{aligned}L = \frac{\omega}{k^2(2 + X)^3\sigma^2}\big[&3(1 + X)(1 + X + X^2)\sigma^2 - 6(1 + X)^2\mu\sigma(\sigma^2 - 1) \\ &+ \mu^2(\sigma^2 - 1)\big((1 + X)^2 + (3 + 2X)\sigma^2\big)\big]\end{aligned} \tag{2.9}$$

and

$$\begin{aligned}N = -\frac{\omega k^2}{8\sigma^2}\Bigg[&\sigma^2\frac{5 + 3X}{2 + X} - \frac{P_0 + P_1X + P_2X^2 + P_3X^3 + X^4}{(3 - \sigma^2 + 3X)(2 + X)} + 2\sigma(2 + X) \\ &\left(\frac{(1 + X)^2 - \sigma^2}{\big(1 - \sigma^2\big)\mu + 3\sigma(1 + X)} + \frac{1 - \sigma^2}{\mu\big(\big(1 - \sigma^2\big) + X(2 + X)\big) + 3\sigma(1 + X)}\right)\Bigg],\end{aligned} \tag{2.10}$$

https://doi.org/10.1017/jfm.2025.10214 Published online by Cambridge University Press

with $\mu = kh$, $\sigma = \tanh\mu$, $X = \sigma\Omega/\omega$ and $P_0 = 21 - 10\sigma^2 + \sigma^4$, $P_1 = 42 + 2\sigma^2 - 4\sigma^4$, $P_2 = 30 + 12\sigma^2$, $P_3 = 9 + 5\sigma^2$.

Note that $|X|$ can be considered as a Strouhal number, which is the ratio between the characteristic frequency of the vorticity and that of the capillary waves.

The coefficients L and N given by (2.9) and (2.10) correspond to those of Hsu *et al.* (2018) for $\kappa = k^2T/(\rho_w g) \to \infty$ and $\Omega \neq 0$ and to those of Djordjevic & Redekopp (1977) in finite depth for $\kappa \to \infty$ and $\Omega = 0$.

The linear dispersion relation of capillary waves in the presence of constant vorticity is

$$\omega^2 + \sigma\Omega\omega - \sigma\frac{k^3T}{\rho_w} = 0. \tag{2.11}$$

From (2.11) it is easy to show that $X > -1$.

As emphasised above, we consider a carrier wave propagating from left to right of frequency ω, phase velocity c_p and group velocity c_g whose expressions are

$$\omega = -\frac{\sigma\Omega}{2} + \sqrt{\left(\frac{\sigma\Omega}{2}\right)^2 + \sigma\frac{k^3T}{\rho_w}}, \tag{2.12}$$

$$c_p = -\frac{\sigma\Omega}{2k} + \sqrt{\left(\frac{\sigma\Omega}{2k}\right)^2 + \sigma\frac{kT}{\rho_w}}, \tag{2.13}$$

$$c_g = -\frac{\Omega h}{2}\left(1-\sigma^2\right) + \frac{\left(1-\sigma^2\right)(\Omega^2 h\sigma/2 + \mu k^2T/\rho_w) + 3\sigma k^2T/\rho_w}{\sqrt{(\Omega\sigma)^2 + 4\sigma k^3T/\rho_w}}. \tag{2.14}$$

2.2. *The Wilton ripple phenomenon and resonant triads*

The nonlinear coefficient N presents two singularities that one should avoid, either

$$3 - \sigma^2 + 3X = 0 \tag{2.15}$$

or

$$\mu\left(\left(1-\sigma^2\right) + X(2+X)\right) + 3\sigma(1+X) = 0. \tag{2.16}$$

Equation (2.15) corresponds to the reduction of the second-harmonic resonance condition of gravity–capillary waves propagating at the free surface of an underlying current of constant vorticity when g goes to zero (κ goes to ∞). This resonance which is also called the Wilton ripple phenomenon occurs when both the fundamental mode and the second harmonic have the same phase velocity, that is, when the phase velocity presents a minimum value. Note that in the absence of positive vorticity ($\Omega < 0$) there is no minimum of phase velocity for pure capillary waves. Martin & Matioc (2013) proved rigorously the existence of Wilton ripples on finite depth for gravity–capillary water waves with constant positive and negative values of the vorticity. The fact that the phenomenon of Wilton ripples for pure capillary waves occurs only for waves propagating from left to right on a current of positive vorticity is a consequence of their lemma 2.5. Using a different approach to investigate the Wilton ripple phenomenon of pure capillary waves our result agrees with that of Martin & Matioc (2013). Note that their study focused on integer values of the wavenumber. The phase velocity c_p reaches a minimal value when $\Omega < 0$ (positive vorticity) and $k = k_m$ given in deep water by

$$k_m = \left(\frac{2\rho_w}{T}\Omega^2\right)^{1/3}. \tag{2.17}$$

https://doi.org/10.1017/jfm.2025.10214 Published online by Cambridge University Press

The wavenumber k satisfying $c_p(k) = c_p(2k)$ is

$$k = \left(\frac{3\rho_w}{4T}\Omega^2\right)^{1/3}. \tag{2.18}$$

The second-harmonic resonance corresponds to the following degenerate resonant triad:

$$2k_1 - k_2 = 0, \tag{2.19}$$

$$2\omega_1 - \omega_2 = 0, \tag{2.20}$$

where

$$\omega_1 = -\frac{\Omega}{2} + \sqrt{\left(\frac{\Omega}{2}\right)^2 + \frac{T}{\rho_w}k^3}, \tag{2.21}$$

$$\omega_2 = -\frac{\Omega}{2} + \sqrt{\left(\frac{\Omega}{2}\right)^2 + \frac{8T}{\rho_w}k^3}, \tag{2.22}$$

with k given by (2.18).

Injecting the expression of k in (2.21) and (2.22), we obtain $\omega_1 = -3\Omega/2$ and $\omega_2 = -3\Omega$.

Constantin & Kartashova (2009) showed that only positive vorticity ($\Omega < 0$) can trigger the occurrence of three-wave resonant interactions of capillary water waves on an underlying current of constant vorticity. As in Martin & Matioc (2013) they considered integer values of the wavenumber. Later on, using the methods of Constantin & Kartashova (2009), Martin (2017) investigated three-wave resonances in deep water to extend their results to gravity–capillary waves. He demonstrated that three-wave resonances of gravity–capillary waves occur only for positive values of the vorticity.

We have shown that the Wilton ripple phenomenon exists in infinite depth for pure capillary waves travelling on a current of constant positive vorticity. To a given fixed value of the vorticity, $-\Omega$, corresponds a resonant real-valued wavenumber given by (2.18); and conversely, to a given fixed real-valued resonant wavenumber, k, corresponds a value of the shear $\Omega = -\sqrt{4Tk^3/(3\rho_w)}$. Fixing $k = 1$ gives the minimal value of the vorticity found by Constantin & Kartashova (2009). Note that within the framework of capillary water waves, the vorticity must be strong to trigger the second-harmonic resonance.

The wavenumber given by (2.18) does not satisfy equation (2.15) unless $\sigma = 1$ that does not mean that there are no second-harmonic resonances in finite depth within the framework of pure capillary waves.

The second singularity corresponds to the reduction of the short-wave/long-wave resonance of gravity–capillary waves propagating at the free surface of an underlying current of constant vorticity when g goes to zero. Note that this singularity disappears in the nonlinear coefficient N when $\sigma = 1$, that is, in deep water. Nevertheless, this does not mean that there are no resonant triad interactions in deep water.

Equation (2.16) has two real-valued negative roots: one is less than -1 and is ruled out because $X > -1$ and the other belongs to $(-1, 0)$ when μ ranges from zero to infinity. It is useful to note that whatever the depth, there exists a singular value of X for $-1 < X < 0$. Constantin & Kartashova (2009) demonstrated that in deep water, capillary waves on a current of positive vorticity ($\Omega < 0$) may give rise to resonant triads.

https://doi.org/10.1017/jfm.2025.10214 Published online by Cambridge University Press

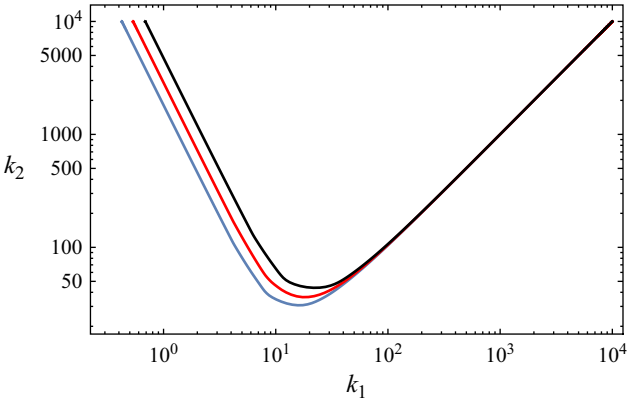


Figure 2. Resonant triad in finite depth: a pair of wavenumbers (k_1, k_2) exciting a third wavenumber $k_3 = k_2 - k_1$. Here $\mu = 1$ (black solid line), $\mu = 0.5$ (red solid line), $\mu = 0.3$ (blue solid line), with $\Omega = -1\ \mathrm{s}^{-1}$ and wavenumbers in m^{-1}.

We found in finite depth triads of capillary waves satisfying the following resonance conditions:

$$k_1 - k_2 + k_3 = 0, \tag{2.23}$$

$$\omega_1 - \omega_2 + \omega_3 = 0, \tag{2.24}$$

with

$$\omega_i = -\frac{\sigma\Omega}{2} + \sqrt{\left(\frac{\sigma\Omega}{2}\right)^2 + \sigma\frac{k_i^3 T}{\rho_w}}, \quad i = 1, 2, 3. \tag{2.25}$$

To illustrate this feature of capillary waves on a current of constant positive vorticity in finite depth, three examples are shown in figure 2 which gives pairs of capillary waves of wavenumbers (k_1, k_2) that excite a third wave of wavenumber k_3. To a given value of k_1 corresponds a value of k_2 and consequently a value of k_3. The three curves present a minimum for the wavenumber k_2.

We can conclude that (2.16) corresponds to resonant triads of capillary waves in finite depth with positive constant vorticity. At any depth, there exists a forbidden positive vorticity value corresponding to a resonant triad.

3. Stability of weakly nonlinear capillary waves on arbitrary depth with constant vorticity

The three-wave interactions are most frequently considered the most likely dominant wave–wave interaction among pure capillary waves. However, Shats, Punzmann & Xia (2010) showed experimentally that the nonlinear four-wave interaction due to modulational instability can be dominant. To shed light on the physical processes governing the formation of steep wave events they considered parametrically excited capillary waves. The new and unexpected finding of their experiments on pure capillary waves was that the dominant wave interaction in the formation of rogue waves is due to modulational instability which is an inseparable feature of the NLS equation that has been used intensively to explain the occurrence of rogue waves. These experiments show the relevance of the study of modulational instability of capillary water waves. Furthermore, the impact of a two-dimensional underlying shear current on these wave–wave interactions is an important issue.

https://doi.org/10.1017/jfm.2025.10214 Published online by Cambridge University Press

Using a Hamiltonian approach, Zakharov (1968) derived in the context of gravity waves on deep water the famous NLS equation and showed that Stokes wave trains are unstable to modulational long-wave perturbations. For a detailed history on the modulational instability the reader may refer to the review paper of Zakharov & Ostrovsky (2009).

The NLS equation (2.8) admits the Stokes wave solution

$$a = a_0 \exp\left(iNa_0^2\tau\right), \tag{3.1}$$

where a is the complex amplitude of the Stokes wave with a_0 real which is the modulus of the complex envelope.

Let us consider an infinitesimal disturbance of this solution so that the perturbed solution is written as follows:

$$a' = a_0\left(1+\delta_a\right)\exp\left(iNa_0^2\tau\right)\exp(i\delta_w). \tag{3.2}$$

Substituting the expression (3.2) of the perturbed solution in the NLS equation (2.8), linearising and separating between real and imaginary parts leads to a system of linear coupled partial differential equations with constant coefficients. Consequently, this system admits solutions of the following forms:

$$\delta_a = (\delta_a)_0 \exp\left(i\left(p\xi - \Gamma\tau\right)\right), \tag{3.3}$$

$$\delta_w = (\delta_w)_0 \exp\left(i\left(p\xi - \Gamma\tau\right)\right), \tag{3.4}$$

where the real p is the perturbation wavenumber.

The necessary and sufficient condition for the existence of a non-trivial solution is

$$\Gamma^2 = p^2\left(L^2p^2 - 2NLa_0^2\right). \tag{3.5}$$

The Stokes wave solution is stable when $L^2p^2 - 2NLa_0^2 \geqslant 0$ and unstable when $L^2p^2 - 2NLa_0^2 < 0$.

The growth rate of instability is

$$\Gamma_i = p\left(2NLa_0^2 - L^2p^2\right)^{1/2}. \tag{3.6}$$

The maximal growth rate of instability is

$$\Gamma_{imax} = \sqrt{\frac{N}{L}}\sqrt{NL}a_0^2, \tag{3.7}$$

for $p = \sqrt{(N/L)}a_0$.

Note that instability occurs when $LN > 0$.

For $\Omega = 0$ the rate of growth of the modulational instability of pure capillary waves on finite depth is

$$\Gamma_i = \frac{\omega}{8k^2}\sqrt{3a_0^2k^4p^2 - 9p^4}, \tag{3.8}$$

which can be found in Chen & Saffman (1985) and Hsu *et al.* (2018). The maximum growth rate is $\omega(a_0k)^2/16$, corresponding to the wavenumber $p_{max} = a_0k^2/\sqrt{6}$.

We introduce dimensionless coefficients $\tilde{L} = k^2L/\omega$ and $\tilde{N} = N/(\omega k^2)$ so that the dispersive and nonlinear coefficients of the NLS equation are functions of $\mu = kh$ and $X = \sigma\Omega/\omega$.

The dimensionless growth rate of instability reads

$$\frac{\Gamma_i}{\omega(a_0k)^2} = \tilde{p}\left(2\tilde{N}\tilde{L} - \tilde{L}^2\tilde{p}^2\right)^{1/2}, \tag{3.9}$$

https://doi.org/10.1017/jfm.2025.10214 Published online by Cambridge University Press

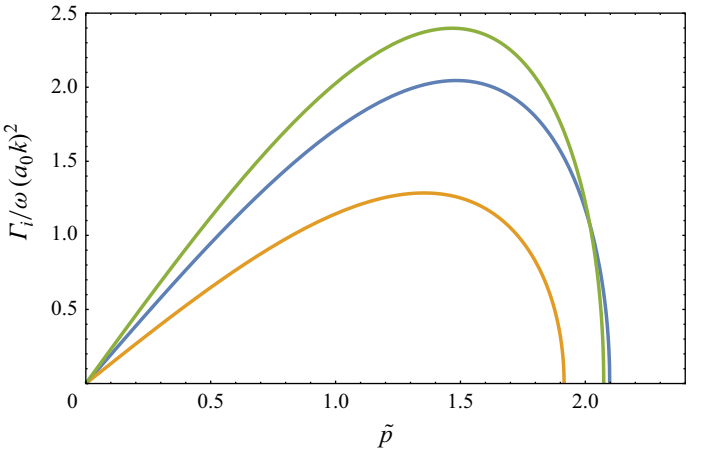


Figure 3. Dimensionless growth rate of instability as a function of the dimensionless perturbation wavenumber for $kh = 0.30$ and $X = -0.40$ (orange solid line), $X = 0$ (blue solid line), $X = 0.40$ (green solid line).

with $\tilde{p} = p/(a_0k^2)$ and its maximal value is

$$\frac{\Gamma_{imax}}{\omega(a_0k)^2} = \sqrt{\frac{\tilde{N}}{\tilde{L}}}\sqrt{\tilde{N}\tilde{L}}, \tag{3.10}$$

for $\tilde{p} = \sqrt{\tilde{N}/\tilde{L}}$.

The dimensionless bandwidth of instability is

$$\Delta\tilde{p} = \sqrt{2\frac{\tilde{N}}{\tilde{L}}}, \quad \frac{\Delta p}{k} = \Delta\tilde{p}\,a_0k. \tag{3.11}$$

The analytic expression of the dimensionless maximal growth rate of instability in deep water reads

$$\frac{\Gamma_{imax}}{\omega(a_0k)^2} = \frac{3 + 14X + 23X^2 + 11X^3 - 3X^4}{24(X+1)(3X+2)}. \tag{3.12}$$

For weak vorticity, (3.12) becomes

$$\frac{\Gamma_{imax}}{\omega(a_0k)^2} = \frac{1}{16}\left(1 + \frac{13}{6}X + \frac{3}{4}X^2\right) + \mathcal{O}(X^3). \tag{3.13}$$

In figures 3 and 4 is plotted the dimensionless growth rate of instability given by (3.9) as a function of the dimensionless perturbation wavenumber $\tilde{p}$ for several values of the depth and vorticity. The dimensionless growth rate of instability increases as the dimensionless shear increases and as the dimensionless vorticity decreases for a given value of the depth. This feature can be observed whatever the depth. For negative dimensionless vorticity, the dimensionless growth rate of instability increases as the depth decreases. This feature is still present in shallow water for positive vorticity. The bandwidth of instability increases as the depth decreases.

Figure 5 shows the dimensionless maximal growth rate of instability as a function of the dimensionless depth, $\mu = kh$, for several values of the dimensionless vorticity. We observe that it starts to increase significantly while $\mu < 2$. In finite and infinite depths, positive

https://doi.org/10.1017/jfm.2025.10214 Published online by Cambridge University Press

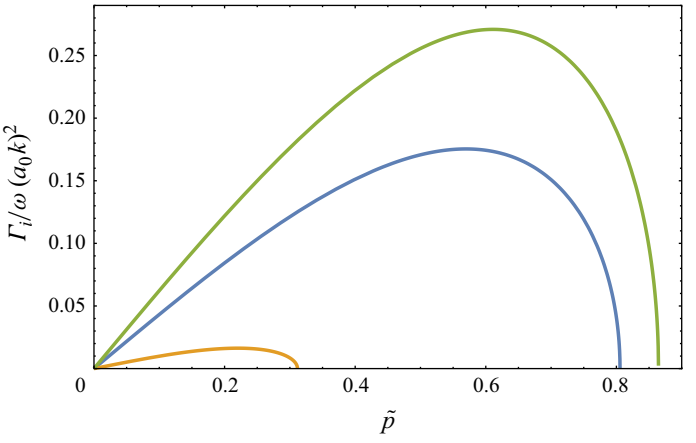


Figure 4. Dimensionless growth rate of instability as a function of the dimensionless perturbation wavenumber for $kh = 1$ and $X = -0.40$ (orange solid line), $X = 0$ (blue solid line), $X = 0.40$ (green solid line).

(negative) dimensionless vorticity increases (reduces) the dimensionless growth rate of instability. In shallow water, this feature persists only for weak dimensionless vorticity.

In figure 6 is plotted the dimensionless maximal growth rate of instability as a function of the vorticity for several values of the dimensionless depth. For about $X < 3$ the dimensionless maximal growth rate of instability increases as the depth decreases, whereas for about $X > 3$ it increases as the depth increases.

Within the framework of irrotational flow ($X = 0$), Tiron & Choi (2012) investigated the stability of the exact deep-water capillary wave solution, derived by Crapper (1957), to two-dimensional infinitesimal disturbances. In figure 7 is plotted the dimensionless growth rate as a function of the dimensionless wavenumber of the modulational perturbation for several values of the wave steepness of the carrier wave. The symbols correspond to the results of Tiron & Choi (2012) whereas the solid line corresponds to the results obtained with the vor-NLS equation. A quite good agreement between the two approaches is obtained when $a_0k \leqslant 0.69$. Note that the maximal wave steepness of Crapper's capillary waves is $a_0k \approx 2.29$.

3.1. *Effect of viscosity and forcing*

The rate of decay of the amplitude of linear waves due to bulk viscosity is $2\nu k^2$, where ν is the kinematic viscosity and k the wavenumber. In the following we consider the modulational instability of capillary waves in the presence of dissipation due to viscosity and some forcing due for instance to wind. Note that this problem has been investigated by Kharif *et al.* (2010) for pure gravity waves in deep water. The latter authors used the Miles mechanism to model wind effect.

Equation (2.8) becomes

$$ia_\tau + La_{\xi\xi} + N|a|^2a = i(\Delta - 2\nu k^2)a, \tag{3.14}$$

where $\Delta > 0$ corresponds to a forcing term.

When $\Delta = 0$, (3.14) is similar to the NLS equation derived rigorously by Dias, Dyachenko & Zakharov (2008) within the framework of weakly damped water waves (see their equation (40)).

https://doi.org/10.1017/jfm.2025.10214 Published online by Cambridge University Press

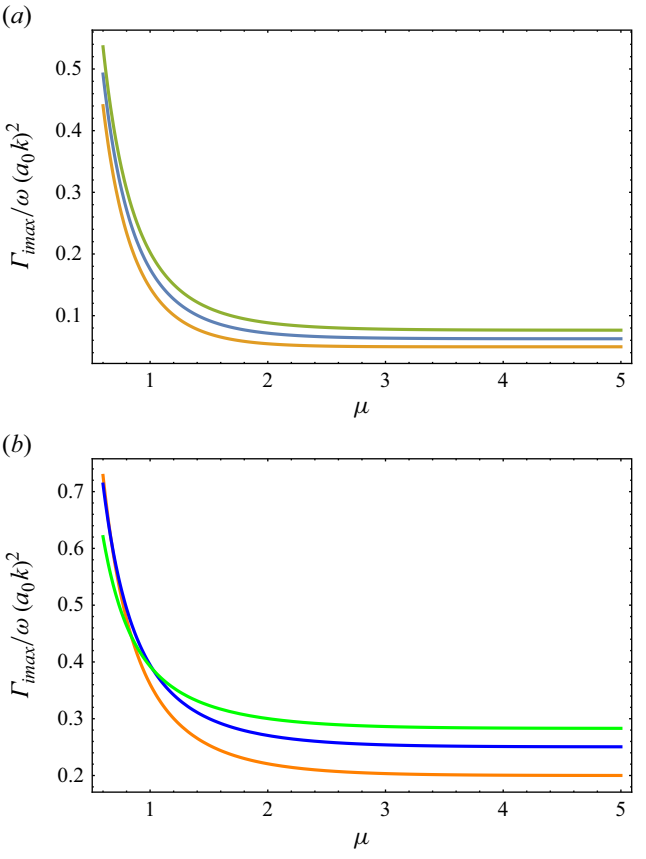


Figure 5. Dimensionless maximal growth rate of instability as a function of the dimensionless depth, $\mu = kh$: (*a*) $X = -0.10$ (orange solid line), $X = 0$ (blue solid line), $X = 0.10$ (green solid line); (*b*) $X = 1$ (orange solid line), $X = 1.5$ (blue solid line), $X = 2$ (green solid line).

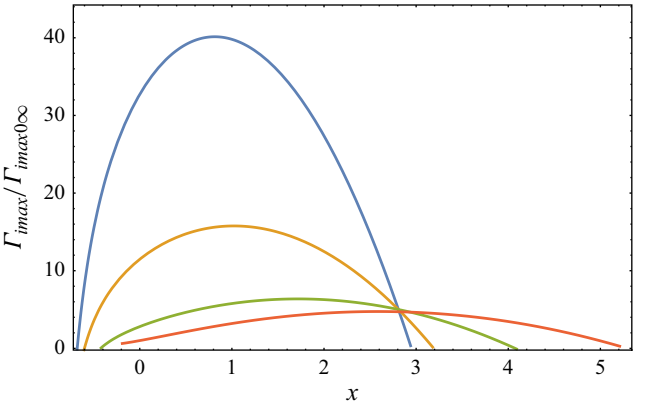


Figure 6. Dimensionless maximal growth rate of instability as a function of the vorticity for several dimensionless depths: $kh = 0.3$ (blue solid line), $kh = 0.5$ (orange solid line), $kh = 1$ (green solid line), $kh = \infty$ (red solid line). Here $\Gamma_{imax0\infty} = \Gamma_{imax}(\Omega = 0,\, kh = \infty)$.

https://doi.org/10.1017/jfm.2025.10214 Published online by Cambridge University Press

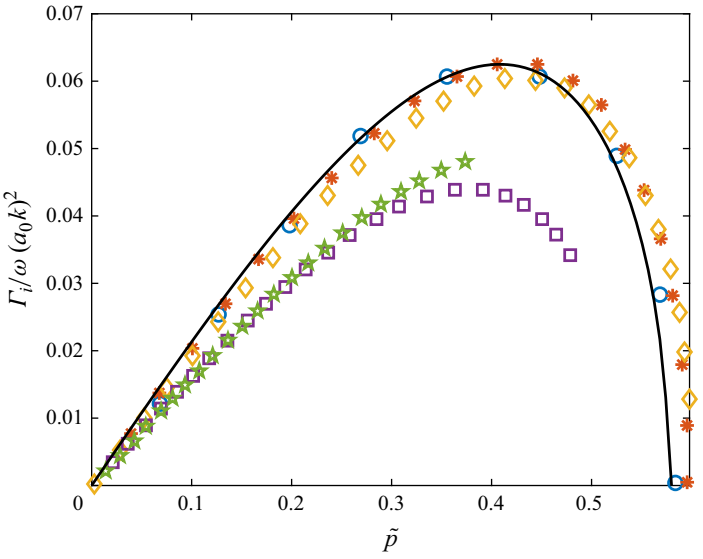


Figure 7. Dimensionless growth rate as a function of the dimensionless perturbation wavenumber in deep water with $X = 0$. Circles, $a_0k = 0.25$; asterisks, $a_0k = 0.47$; diamonds, $a_0k = 0.69$; squares, $a_0k = 1.03$; stars, $a_0k = 1.16$. The symbols correspond to the results of Tiron & Choi (2012) and the solid line corresponds to those of the vor-NLS equation.

Equation (3.14) admits the following solution:

$$a_s = a_0 \exp(K\tau) \exp\left(\frac{iN}{2K} a_0^2 \left(e^{2K\tau} - 1\right)\right), \tag{3.15}$$

where $K = \Delta - 2\nu k^2$.

Note that a_s is spatially constant.

We superimpose to this solution a small disturbance:

$$a(\xi, \tau) = a_s(1 + \epsilon a'(\xi, \tau)), \tag{3.16}$$

with $\epsilon \ll 1$.

Substituting (3.16) into (3.14) and keeping only terms of order ϵ and separating the real and imaginary parts of $a'(\xi, \tau) = a'_r(\xi, \tau) + ia'_i(\xi, \tau)$ gives

$$a'_{i\tau} - La'_{r\xi\xi} - 2Na_0^2 \exp(2K\tau) a'_r = 0, \tag{3.17}$$

$$a'_{r\tau} + La'_{i\xi\xi} = 0. \tag{3.18}$$

Set $a'_r(\xi, \tau) = \mathrm{Re}(a'_{r0}(\tau) \exp(ip\xi))$ and $a'_i(\xi, \tau) = \mathrm{Im}(a'_{i0}(\tau) \exp(ip\xi))$, where p is the wavenumber of the perturbation. Then,

$$\frac{\mathrm{d}a'_{i0}}{\mathrm{d}\tau} + \left(Lp^2 - 2Na_0^2 \exp(2K\tau)\right) a'_{r0} = 0, \tag{3.19}$$

$$\frac{\mathrm{d}a'_{r0}}{\mathrm{d}\tau} - Lp^2 a'_{i0} = 0. \tag{3.20}$$

Combining the two previous equations gives

$$\frac{d^2 a'_{r0}}{\mathrm{d}\tau^2} + L^2 p^4 \left(1 - \frac{2N}{Lp^2} a_0^2 \exp(2K\tau)\right) a'_{r0} = 0. \tag{3.21}$$

One may distinguish two cases according to whether K is negative or positive.

https://doi.org/10.1017/jfm.2025.10214 Published online by Cambridge University Press

(i) Let K be negative. This case was analysed by Segur, Henderson & Carter (2005) and Kharif *et al.* (2010). In the presence of damping, the modulational instability is stabilised by viscous dissipation. However, note that the modulational instability may grow, but its growth is limited and starts to stabilise after a time $\tau = -(1/2K)\ln(2Na_0^2/Lp^2)$ corresponding to the change of sign of the coefficient of a'_{r0} of (3.21). Note that the bandwidth of instability shrinks as the amplitude of the carrier wave diminishes, resulting in stabilisation of unstable modes. The most unstable perturbation starts stabilisation at $\tau = \ln 2/(4\nu k^2)$. Let us consider a carrier wave of wavelength $\lambda = 0.005$ m in deep water. For $X = 0$, stabilising of the most unstable perturbation will start at $\tau \approx 7\tau_0$, where τ_0 is the dimensional period of the carrier wave. For $X = 0.4$ and $X = -0.4$, we found that the most unstable perturbation stabilises at $\tau \approx 6\tau_0$ and $\tau \approx 9\tau_0$, respectively. These critical times are more or less confirmed by numerical simulations of dimensionless equation (3.24) (see figure 8) without forcing.

(ii) Let K be positive. This case was discussed by Kharif *et al.* (2010) who considered gravity wave trains on the surface of water acted upon by wind and under the influence of viscosity. Herein, a similar situation is considered within the framework of pure capillary wave trains. In this case, the modulational perturbations are initially oscillating for $0 < \tau < (1/2K)\ln(2Na_0^2/Lp^2)$ and then start to grow exponentially for $\tau > (1/2K)\ln(2Na_0^2/Lp^2)$. The bandwidth of instability increases as the amplitude of the carrier wave increases. Consequently, stable modes may become unstable. Let p be a perturbation wavenumber corresponding to a stable state. There is a critical value of the carrier wave amplitude, a_0, for which the bandwidth instability is equal to p. For carrier wave amplitude larger than this critical value, the perturbation becomes unstable. The critical value is given by $\Gamma_i = 0$, that is to say,

$$a_{0c}^2 = \frac{Lp^2}{2N}. \tag{3.22}$$

The modulational instability will start to grow as soon as the carrier wave amplitude reaches the critical value. When the carrier wave amplitude is set equal to a_{0c}, the instability starts at $\tau = 0$.

Let us consider the case without vorticity ($X = 0$) in deep water. The dispersive and nonlinear coefficients of the vor-NLS equation are $L = 3\omega/(8k^2)$ and $\omega k^2/16$. The critical wave steepness of the carrier wave is

$$a_{0c}k = \sqrt{3}\, p/k. \tag{3.23}$$

This critical value is more or less confirmed by numerical simulations of dimensionless equation (3.24) (see figure 9*a*) with forcing, $\tilde{K} = (\tilde{\Delta} - 2/R_e)$.

For $(X,\ p/k) = (0.4,\ 0.72)$ and $(X,\ p/k) = (-0.4,\ 0.59)$ we found, in deep water, $a_{0c}k \approx 1$ and 1.5, respectively (see figure 9*b*,*c*).

To complete the linear stability analysis, we consider the nonlinear evolution of unstable and stable modes. To do this, we use (3.14) written in dimensionless form with respect to the reference length $1/k$ and reference time $1/\omega$, where k and ω are the wavenumber and frequency of the carrier wave, respectively:

$$i\tilde{a}_{\tilde{\tau}} + \tilde{L}\tilde{a}_{\tilde{\xi}\tilde{\xi}} + \tilde{N}|\tilde{a}|^2\tilde{a} = i\left(\tilde{\Delta} - \frac{2}{R_e}\right)\tilde{a}, \tag{3.24}$$

https://doi.org/10.1017/jfm.2025.10214 Published online by Cambridge University Press

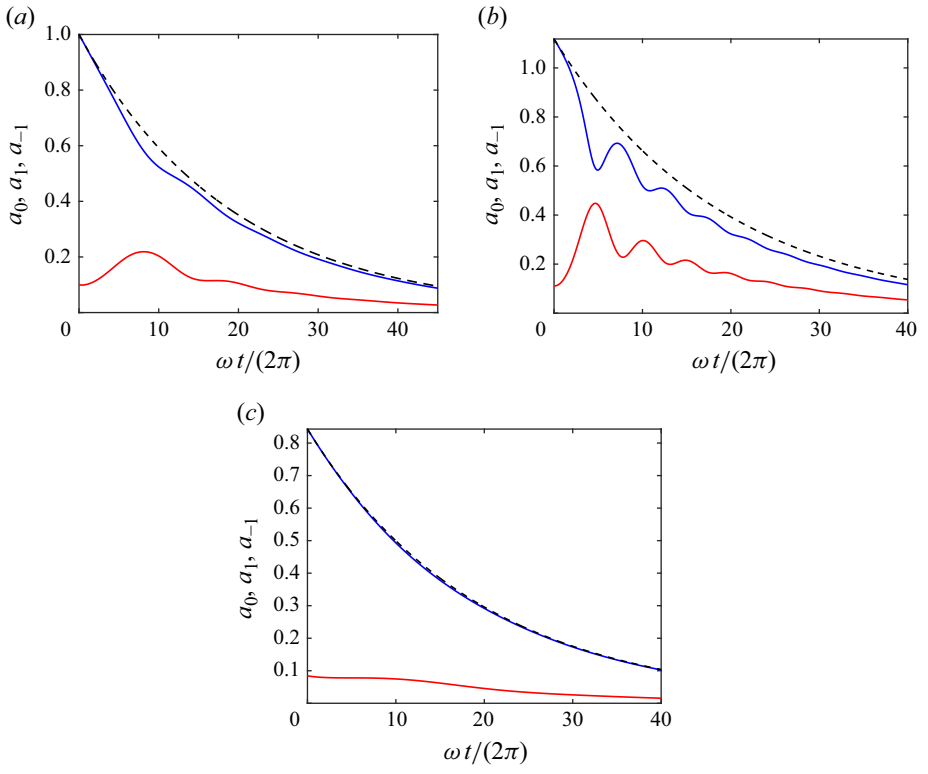


Figure 8. Temporal evolution of the dimensionless amplitudes of the carrier wave (solid blue line) and most unstable sideband modes (solid red line) in the presence of viscous dissipation in deep water: (*a*) $X = 0$, $R_e \approx 240$; (*b*) $X = 0.4$, $R_e \approx 202$; (*c*) $X = -0.4$, $R_e \approx 308$. Herein, $\omega = 1$.

where $R_e = \omega/(k^2\nu)$.

Within the framework of numerical simulations of the vor-NLS equation, figure 8 shows, in the presence of viscous dissipation only and for several values of the vorticity, the temporal evolution of the amplitude of the carrier wave, a_0, and those of the most unstable sidebands, a_{-1} and a_{+1}, whose curves overlap. At the beginning of the nonlinear interaction, the modulational instability is growing due to a transfer of energy from the carrier wave to the sidebands and then stabilises under the effect of the dissipation (see figure 8*a*,*b*). The case corresponding to figure 8(*c*) presents a different behaviour because the initial rate of growth of the instability and the rate of damping are of the same order, preventing the instability from developing.

Figure 9 shows, in the presence of forcing assumed to be a constant, the temporal evolution of the amplitude of the carrier wave, a_0, and those of the initially stable sidebands, a_{-1} and a_{+1}, for several values of the vorticity. At the beginning, numerical simulations show that the perturbations are oscillating and then are growing.

4. Capillary solitary waves on deep water in the presence of constant vorticity

Equation (2.8) admits as solution the envelope soliton given by the following expression:

$$a(\xi, \tau) = \pm a_0 \operatorname{sech}\left(a_0 \left(\frac{N}{2L}\right)^{1/2} \xi\right) \exp(iNa_0^2\tau/2). \tag{4.1}$$

https://doi.org/10.1017/jfm.2025.10214 Published online by Cambridge University Press

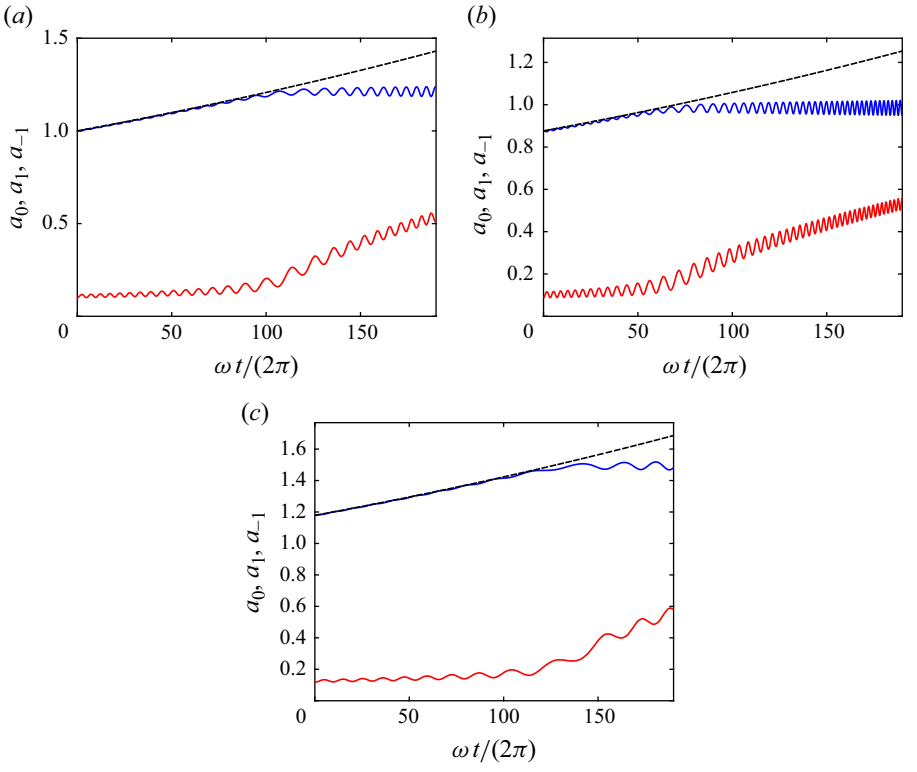


Figure 9. Temporal evolution of the dimensionless amplitudes of the carrier wave (solid blue line) and stable sideband modes (solid red line) in the presence of weak forcing in deep water: (*a*) $X = 0$, $p/k = 0.7$; (*b*) $X = 0.4$, $p/k = 0.72$; (*c*) $X = -0.4$, $p/k = 0.59$; $\tilde{K} = 3/10\,000$. Herein, $\omega = 1$.

The corresponding surface elevation of a weakly nonlinear wave train of envelope given by (4.1) is

$$\zeta = \pm\frac{1}{2}\epsilon a_0 \,\mathrm{sech}\left(\sqrt{\frac{N}{2L}}\, a_0\epsilon(x - c_g t)\right)\exp\left(ikx - i\left(\omega - \frac{N}{2}\epsilon^2 a_0^2\right)t\right) + \text{c.c.}, \quad (4.2)$$

where k and ω are the carrier wavenumber and carrier frequency and c.c. is the complex conjugation.

Near the minimum of phase velocity of linear gravity–capillary waves, the phase velocity and the group velocity are nearly equal. As stated by Longuet-Higgins (1993) in any dispersive medium supporting an envelope soliton and whose linear dispersion has an extremum we can expect that steady solitary waves with decaying oscillatory tails bifurcate from linear periodic waves. These waves are called generalised solitary waves to distinguish them from those which are flat at $x = \pm\infty$. For a review on this problem, the reader is referred to Dias & Kharif (1999). It is noteworthy to emphasise that a pure periodic capillary wave train can bifurcate into generalised solitary waves only in the presence of positive vorticity as mentioned in § 2. Bifurcation cannot occur for negative vorticity because there is no phase velocity minimum.

Following Akylas (1993) and Abid *et al.* (2019) we consider a train of periodic pure capillary waves on deep water bifurcating into a solitary wave with a decaying oscillatory tail in the presence of positive vorticity ($\Omega < 0$). Note that Akylas (1993) and Abid *et al.* (2019) considered gravity–capillary waves.

https://doi.org/10.1017/jfm.2025.10214 Published online by Cambridge University Press

We use $T/(\rho_w c^2)$ and $T/(\rho_w c^3)$ as unit of length and unit of time, where c is the phase velocity of the envelope soliton. In this way c is the reference phase velocity scale. Note that this normalisation is equivalent to setting $T = 1$, $\rho_w = 1$ and $c = 1$.

Within the framework of the new normalisation, the condition for the envelope soliton to be a solitary is

$$\omega(k, \Omega) - \frac{1}{2} N a_0^2 \epsilon^2 = k, \quad \frac{\partial \omega}{\partial k} = 1. \tag{4.3}$$

Critical values of the parameters are obtained by setting $\epsilon = 0$ in (4.3):

$$k_0 = \omega(k_0, \Omega_0), \quad \frac{\partial \omega}{\partial k}(k_0, \Omega_0) = 1. \tag{4.4}$$

Solving these two equations gives

$$k_0 = \frac{1}{2}, \quad \Omega_0 = -\frac{1}{4}, \quad \omega_0 = \frac{1}{2}. \tag{4.5}$$

The carrier wavenumber k and the shear Ω are expanded about (k_0, Ω_0) as follows:

$$k = k_0 + k_1 \epsilon^2 + \mathcal{O}(\epsilon^3), \tag{4.6}$$

$$\Omega = \Omega_0 + \Omega_1 \epsilon^2 + \mathcal{O}(\epsilon^3). \tag{4.7}$$

Expanding $\omega(k, \Omega)$ about (k_0, Ω_0) and using

$$k = \omega(k, \Omega) - \frac{1}{2} N \epsilon^2 a_0^2, \tag{4.8}$$

with $\partial\omega/\partial k(k_0, \Omega_0) = 1$, gives

$$\Omega_1 = \frac{1}{2} \frac{N(k_0, \Omega_0)}{\dfrac{\partial \omega}{\partial \Omega}(k_0, \Omega_0)} a_0^2, \tag{4.9}$$

$$k_1 = -\frac{\dfrac{\partial^2 \omega}{\partial k \partial \Omega}(k_0, \Omega_0)}{2L(k_0, \Omega_0)} \Omega_1. \tag{4.10}$$

Let $\delta\Omega$ be the difference between Ω and the critical value Ω_0:

$$\delta\Omega = \Omega_1 \epsilon^2 + \mathcal{O}(\epsilon^3). \tag{4.11}$$

The square of the amplitude of the generalised solitary wave is

$$a_0^2 \epsilon^2 = 2 \frac{\dfrac{\partial \omega}{\partial \Omega}(k_0, \Omega_0)}{N(k_0, \Omega_0)} \delta\Omega \tag{4.12}$$

and

$$k = k_0 - \frac{\dfrac{\partial^2 \omega}{\partial k \partial \Omega}(k_0, \Omega_0)}{2L(k_0, \Omega_0)} \delta\Omega. \tag{4.13}$$

Substituting the critical values given by (4.5) into (4.12) and (4.13) gives

$$a_0^2 \epsilon^2 = -\frac{32^2}{3} \delta\Omega, \quad \delta\Omega < 0, \tag{4.14}$$

$$k = k_0 - \frac{3}{16} \delta\Omega, \quad \delta\Omega < 0. \tag{4.15}$$

https://doi.org/10.1017/jfm.2025.10214 Published online by Cambridge University Press

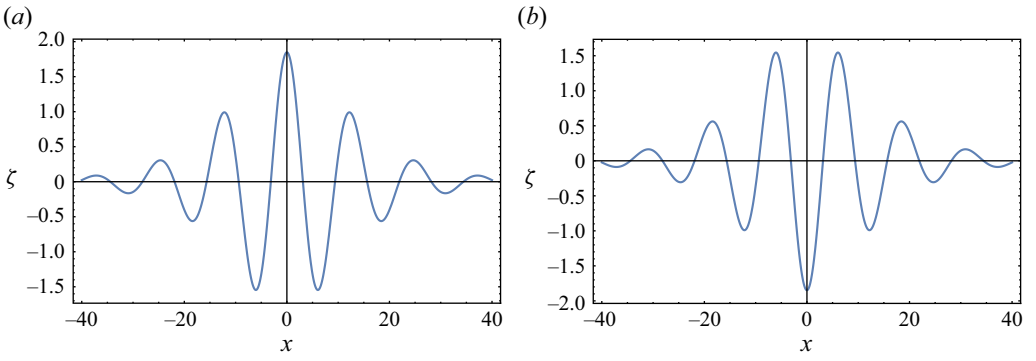


Figure 10. Dimensionless profiles of generalised capillary solitary waves of elevation (*a*) and depression (*b*) in deep water for $\delta\Omega = -0.01$.

Consequently, the profile of the generalised solitary wave is

$$\zeta(x,t) = \pm\frac{32}{\sqrt{3}}\sqrt{-\delta\Omega}\,\operatorname{sech}\left(\sqrt{-\delta\Omega}(x-t)\right)\cos\left(k(x-t)\right). \tag{4.16}$$

The profile of the generalised solitary wave is known once the bifurcation parameter $\delta\Omega$ is fixed. At $\Omega = \Omega_0$ the train of linear periodic capillary waves bifurcates into a solitary wave whose profile is given by (4.16). The (+) sign corresponds to a generalised solitary wave of elevation, whereas the (−) sign corresponds to a generalised solitary wave of depression.

The envelope soliton is unstable to transverse perturbations (see § 5). Consequently, capillary solitary waves with decaying oscillatory tails are expected to be unstable, too.

Within the framework of irrotational flow, Ifrim & Tataru (2020) proved rigorously that there are no capillary solitary waves in deep water with a free surface asymptotically flat at infinity. We have shown that capillary solitary waves with decaying oscillatory tails in the presence of constant positive vorticity may exist in deep water. Within the framework of rotational flows, we have shown that generalised capillary solitary waves may exist. In figures 10 and 11 are plotted the dimensionless profiles of generalised capillary solitary waves in deep water for two values of the bifurcation parameter $\delta\Omega$. The profiles become flatter when $|\delta\Omega|$ increases. This feature could suggest the existence of capillary solitary waves being flat in the far field at the free surface of rotational flows of positive vorticity in deep water.

5. Transverse instability of the capillary envelope soliton and capillary Stokes wave in deep water with constant vorticity

Within the framework of deep water, Ellingsen (2016) showed that a wave of weak amplitude can propagate at an angle on a vertically sheared current without introducing additional vorticity, if the vorticity is also weak. He also emphasised that this claim can be applied to linear waves propagating in finite depth (Ellingsen 2014). Consequently, results presented in the following two subsections concern capillary waves travelling on a shear current of weak vorticity.

In the two following subsections, we consider the stability of the capillary envelope soliton and capillary Stokes waves to transverse perturbations. Note that the vorticity of the underlying current is now perturbed by the infinitesimal periodic vorticity due to the

https://doi.org/10.1017/jfm.2025.10214 Published online by Cambridge University Press

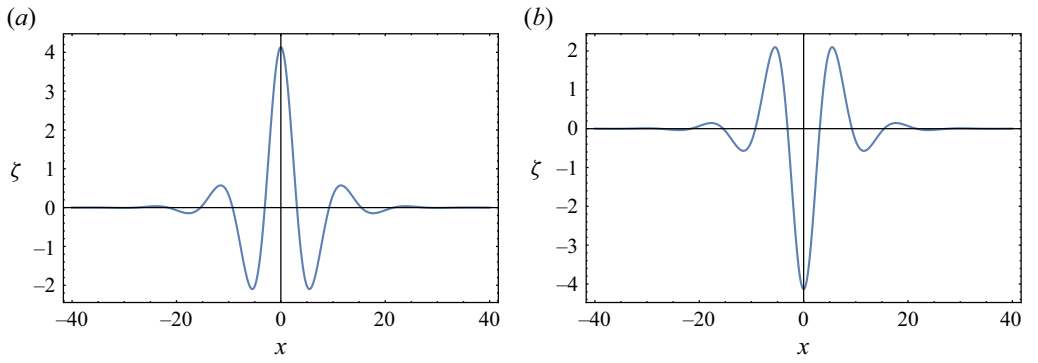


Figure 11. Dimensionless profiles of generalised capillary solitary waves of elevation (a) and depression (b) in deep water for $\delta\Omega = -0.05$.

perturbation, while in one-dimensional propagation the perturbation is potential and does not affect the shear. Nevertheless, the phase average of the vorticity is $-\Omega$.

5.1. *Capillary envelope soliton*

In two dimensions the NLS equation in deep water reads

$$ia_\tau + La_{\xi\xi} + Ma_{\eta\eta} + N|a|^2 a = 0, \tag{5.1}$$

with

$$L = \frac{3\omega}{k^2}\left(\frac{(1+X)(1+X+X^2)}{(2+X)^3}\right), \tag{5.2}$$

$$N = \frac{\omega k^2}{24}\left(\frac{3+14X+23X^2+11X^3-3X^4}{(X+1)(3X+2)}\right), \tag{5.3}$$

$$M = \frac{3T}{2\rho_w}\left(\frac{k}{\omega(2+X)}\right). \tag{5.4}$$

Here in $X = \Omega/\omega$.

Equation (5.1) admits as solution the two-dimensional envelope soliton, $\bar{a}(\xi, \tau)$, given by (4.1). We consider the stability of this solution to infinitesimal disturbances:

$$a(\xi, \eta, \tau) = \bar{a}(\xi, \tau) + a'(\xi, \eta, \tau)\exp\left(iNa_0^2\tau/2\right). \tag{5.5}$$

The stability analysis is similar to that used by Abid *et al.* (2019) for gravity–capillary envelope soliton, except that now the coefficients of the NLS equation correspond to pure capillary envelope soliton. Linearisation of (5.1) about $\bar{a}$ with $a' = u + iv$ gives

$$v_\tau = Lu_{\xi\xi} + Mu_{\eta\eta} + \left(3NA^2 - Na_0^2/2\right)u, \tag{5.6}$$

$$u_\tau = -Lv_{\xi\xi} - Mv_{\eta\eta} - \left(NA^2 - Na_0^2/2\right)v, \tag{5.7}$$

where

$$A = a_0\,\mathrm{sech}\left(a_0\left(\frac{N}{2L}\right)^{1/2}\xi\right). \tag{5.8}$$

https://doi.org/10.1017/jfm.2025.10214 Published online by Cambridge University Press

The system (5.6)–(5.7) of linear partial differential equations with constant coefficients admits solutions of the following form:

$$u = \hat{u}(\xi)\exp(iq\eta + \Gamma\tau), \tag{5.9}$$

$$v = \hat{v}(\xi)\exp(iq\eta + \Gamma\tau). \tag{5.10}$$

Substitution of (5.9) and (5.10) into (5.6) and (5.7) gives

$$\Gamma\hat{v} = L\frac{d^2\hat{u}}{\mathrm{d}\xi^2} - Mq^2\hat{u} + \left(3NA^2 - Na_0^2/2\right)\hat{u}, \tag{5.11}$$

$$\Gamma\hat{u} = -L\frac{d^2\hat{v}}{\mathrm{d}\xi^2} + Mq^2\hat{v} - \left(NA^2 - Na_0^2/2\right)\hat{v}. \tag{5.12}$$

The eigenfunction $\hat{v}$ can be eliminated:

$$\Gamma^2\hat{u} = -\left(D_0 - Mq^2\right)\left(D_1 - Mq^2\right)\hat{u}, \tag{5.13}$$

with

$$D_0 = L\frac{d^2}{\mathrm{d}\xi^2} + NA^2 - Na_0^2/2, \tag{5.14}$$

$$D_1 = L\frac{d^2}{\mathrm{d}\xi^2} + 3NA^2 - Na_0^2/2. \tag{5.15}$$

The eigenfunction $\hat{u} \to 0$ as $\xi \to \infty$ (the eigenfunctions are local in ξ). Note that the non-local states corresponding to the continuum spectrum are stable or marginally stable (Saffman & Yuen 1978; Rypdal & Rasmussen 1989). Zakharov & Rubenchik (1974) investigated analytically the transverse instability of envelope solitons.

The numerical method used to solve (5.13) is outlined in Appendix A of Abid *et al.* (2019).

Without loss of generality, we set $T = 1$, $\rho_w = 1$ and $k = 1$ as in Saffman & Yuen (1985) and Tiron & Choi (2012). For the sake of clarity, the same symbols are used for the coefficients of the NLS equation. For comparison, we consider the analytic expression of the instability growth rate derived by Rypdal & Rasmussen (1989) and Abid *et al.* (2019), given in dimensionless form by

$$\Gamma^2 = \frac{32}{\pi^2}MNq^2\left(1 - \frac{M}{3N}q^2\right), \tag{5.16}$$

$$\Gamma_{max}^2 = \frac{24}{\pi^2}N^2, \tag{5.17}$$

with

$$q_{max} = \sqrt{\frac{3N}{2M}}. \tag{5.18}$$

The capillary envelope soliton is unstable to infinitesimal transverse perturbations of wavenumber q satisfying $q^2 < 3N/M$. Figure 12 shows the square of the dimensionless growth rate as a function of the square of the dimensionless transverse wavenumber for different values of the vorticity. The numerical and analytical results are in excellent agreement. The dimensionless growth rate and instability bandwidth increase as the

https://doi.org/10.1017/jfm.2025.10214 Published online by Cambridge University Press

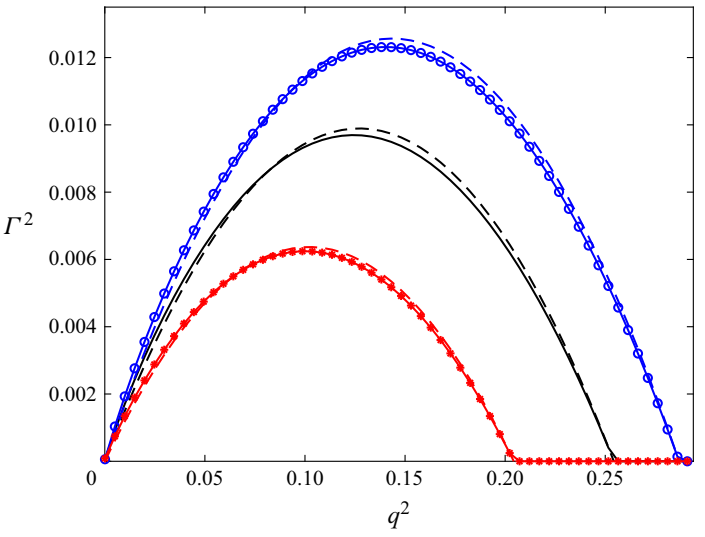


Figure 12. Square of the dimensionless growth rate of the transverse unstable mode of capillary envelope soliton in deep water as a function of the square of the dimensionless wavenumber for $X = -0.1$ (stars), $X = 0$ (solid line), $X = 0.1$ (circles). The dashed lines correspond to the analytical expression given by (5.16).

dimensionless vorticity decreases. Note that in deep water

$$\Omega^2 = \frac{Tk^3}{\rho_w}\frac{X^2}{1+X} \quad \text{with } X > -1, \tag{5.19}$$

and in dimensionless form

$$\Omega^2 = \frac{X^2}{1+X}. \tag{5.20}$$

5.2. *Capillary Stokes waves*

Equation (5.1) admits as solution the Stokes wave envelope given by (3.1). This solution is unstable to perturbations of longitudinal and transverse wavenumbers p and q if

$$Lp^2 + Mq^2 < 2Na_0^2. \tag{5.21}$$

Using the linear dispersion (2.11) the coefficient M is rewritten as follows:

$$M = \frac{3\omega}{2k^2}\frac{1+X}{2+X}. \tag{5.22}$$

In a more explicit form, condition (5.21) reads

$$\frac{3(1+X)(1+X+X^2)}{(2+X)^3}p^2 + \frac{3(1+X)}{2(2+X)}q^2 < \frac{3+14X+23X^2+11X^3-3X^4}{12(1+X)(2+3X)}a_0^2k^4. \tag{5.23}$$

The instability condition $p^2 + 2q^2 < k^4a_0^2/3$, established by Chen & Saffman (1985), is recovered for $X = 0$.

The square of growth rate of instability is

$$\Gamma_i^2 = \left(Lp^2 + Mq^2\right)\left(2Na_0^2 - Lp^2 - Mq^2\right). \tag{5.24}$$

https://doi.org/10.1017/jfm.2025.10214 Published online by Cambridge University Press

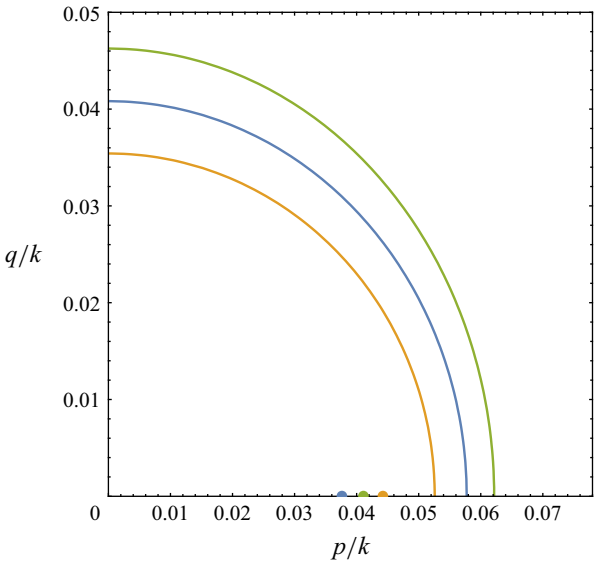


Figure 13. Infinite-depth stability diagram in the $(p/k, q/k)$ plane for $a_0k = 0.1$ and three values of the vorticity. Blue: $X = 0$; orange: $X = -0.1$; green: $X = 0.1$. Dots correspond to the maximal growth rate of instability.

Substituting the expressions of L, M and N into (5.24), we obtain in dimensionless form

$$\frac{\Gamma_i^2}{\omega^2} = \frac{3(1+X)}{2+X}\left(\frac{1+X+X^2}{(2+X)^2}\frac{p^2}{k^2} + \frac{q^2}{2k^2}\right) \times \left(\frac{3+14X+23X^2+11X^3-3X^4}{12(1+X)(2+X)}a_0^2k^2 - \frac{3(1+X)}{2+X}\left(\frac{1+X+X^2}{(2+X)^2}\frac{p^2}{k^2} + \frac{q^2}{2k^2}\right)\right). \tag{5.25}$$

For $X = 0$ we recover the growth rate of instability of Chen & Saffman (1985) given by

$$\Gamma_i = \frac{1}{8}\left(3a_0^2k^3\left(p^2+2q^2\right) - \frac{9}{k}\left(p^2+2q^2\right)^2\right)^{1/2}. \tag{5.26}$$

Note that Chen & Saffman (1985) used the relation $\omega^2 = k^3$.

The boundary of the stability diagram in the $(p/k, q/k)$ plane is given by the following ellipse equation:

$$\frac{(1+X+X^2)}{(2+X)^2}\left(\frac{p}{k}\right)^2 + \frac{1}{2}\left(\frac{q}{k}\right)^2 = \frac{3+14X+23X^2+11X^3-3X^4}{36(1+X)^2}a_0^2k^2. \tag{5.27}$$

Within the framework of deep water, figure 13 shows the stability diagram in the $(p/k, q/k)$ plane for three values of the dimensionless vorticity. The domain of instability increases as the vorticity decreases. Dots plotted in the figure, located on the p axis, correspond to the dimensionless maximal growth rate of modulational instability. Consequently, the dominant modulational instability of weakly nonlinear capillary waves on deep water is two-dimensional. The wavelength of the dominant modulational instability increases as the vorticity decreases. For $\Omega = 0$ we found $p/k = 0.0416$ which is very close to the value obtained by Chen & Saffman (1985) in their table 1.

https://doi.org/10.1017/jfm.2025.10214 Published online by Cambridge University Press

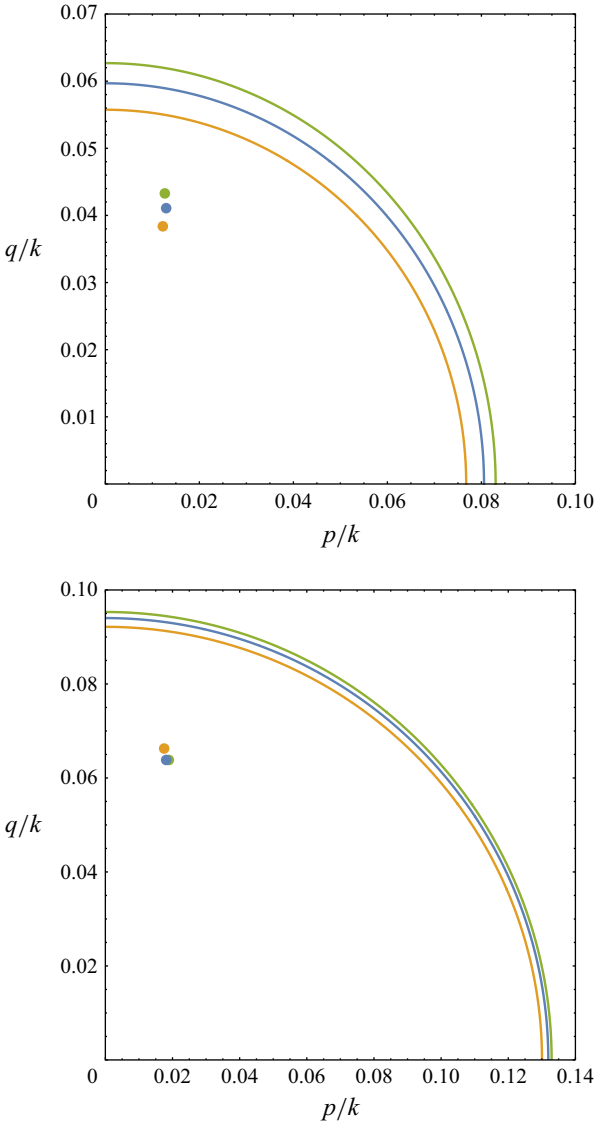


Figure 14. Plots for (*a*) $kh = 1$ and (*b*) $kh = 0.5$. Blue: $X = 0$; orange: $X = -0.1$; green: $X = 0.1$. Dots correspond to the maximal growth rate of instability.

Figure 14 shows the stability diagram in the $(p/k, q/k)$ plane in finite depth for $kh = 0.5$ and $kh = 1$ and three values of vorticity. The most unstable perturbation is three-dimensional in contrast to two-dimensional perturbations, which are dominant instabilities in deep water. Note that within the framework of gravity waves McLean (1982*a*,*b*) showed that the most unstable perturbation is two-dimensional in deep water whereas it is three-dimensional in finite depth.

In figure 15 is plotted the dimensionless maximal growth rate as a function of the dispersive parameter kh: the dimensionless maximal growth rate decreases as kh increases.

https://doi.org/10.1017/jfm.2025.10214 Published online by Cambridge University Press

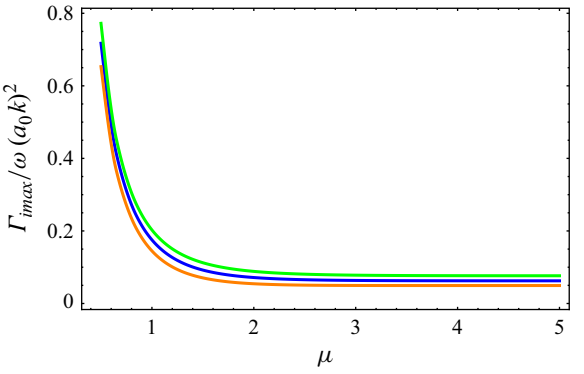


Figure 15. Dimensionless maximal growth rate of oblique instability as a function of the dimensionless depth, $\mu = kh$: $X = -0.10$ (orange solid line), $X = 0$ (blue solid line), $X = 0.10$ (green solid line).

6. Conclusion

A NLS equation for pure capillary waves on arbitrary depth with a shear current of constant vorticity has been derived, which completes the previous works of Thomas *et al.* (2012) and Hsu *et al.* (2018) on gravity waves and gravity–capillary waves, respectively.

We have shown that the Wilton ripple phenomenon exists in infinite depth for pure capillary waves propagating on a current of constant positive vorticity and that the second singularity of the nonlinear coefficient of the vor-NLS equation corresponds to resonant triads of capillary waves in finite depth with positive vorticity.

The influence of the vorticity on the modulational instability of weakly nonlinear capillary waves on arbitrary depth has been investigated in detail. We found that the dimensionless growth rate of modulational instability increases as the dimensionless vorticity decreases whatever the dispersive parameter, kh, where k is the carrier wavenumber and h the depth. The dimensionless maximal growth rate is strongly amplified for shallow water depths. The dimensionless bandwidth of instability increases as the dimensionless vorticity decreases.

To measure the effect of bulk viscosity on the modulational instability of pure capillary waves travelling on a current of constant vorticity, we have considered the damped vor-NLS equation. The linear stability analysis reduces to a Sturm–Liouville problem. We found that the most unstable perturbation stabilises faster for negative vorticity and later for positive vorticity. This was confirmed by numerical simulations of the damped vor-NLS equation in deep water. In the presence of a forcing term, we have used the forced vor-NLS equation. We found that a stable perturbation will become unstable as soon as the carrier wave amplitude reaches a critical value, which depends on the vorticity and the wavenumber of the perturbation. Furthermore, a stability analysis of weakly nonlinear capillary waves, in deep water and finite depth, to transverse perturbations has shown that the dominant modulational instability is two-dimensional in deep water whereas the dominant instability is three-dimensional in finite depth.

Within the framework of rotational flows of positive vorticity, we have shown, near the minimum of phase velocity of linear capillary waves on deep water, that generalised capillary solitary waves bifurcate from linear periodic capillary waves.

We investigated the linear stability of the envelope soliton of pure capillary waves to transverse perturbation in deep water. We found that the dimensionless growth rate and instability bandwidth increase as the dimensionless vorticity decreases.

https://doi.org/10.1017/jfm.2025.10214 Published online by Cambridge University Press

Funding. This research received funding from the Centre National d'Études Spatiales (CNES), under grant CNES OTP 60115, 2023-2026, for the project CROSSEAS.

Declaration of interests. The authors report no conflict of interest.

Data availability statement. The data that support the findings of this study are available upon request.

Author contributions. C.K.: Formal analysis; Investigation; Project administration; Methodology; Validation; Writing. M.A.: Formal analysis; Investigation; Project administration; Software; Validation; Visualisation; Writing; Data curation. Y.-Y.C.: Formal analysis; Project administration. H.-C.H.: Formal analysis; Project administration.

Appendix

The expression of the nonlinear coefficient given by Hsu *et al.* (2018) is rewritten as follows:

$$
\begin{aligned}
N = &-\frac{\omega k^2}{8\sigma^2(1+X)(2+X)}\left[\sigma^2(1+X)\left(8+6X-3(1+X)\frac{\kappa}{1+\kappa}\right)\right.\\
&-2\left(1-\sigma^2\right)\left[(1+X)^2-\sigma^2\right](1+\kappa)+\frac{1+X}{\sigma^2-\kappa(3-\sigma^2+3X)}N_1\\
&+\frac{2\rho\left(1-\sigma^2\right)+2(1+X)(2+X)}{\rho^2+\mu\rho\dfrac{X}{\sigma}-\dfrac{\mu(1+X)}{\sigma(1+\kappa)}}\left(\left(\rho+\mu\frac{X}{\sigma}\right)\left((1+X)^2-\sigma^2\right)+(1+X)(2+X)\right)\\
&\left.-\frac{2(1+X)^2(2+X)^2}{\rho^2+\mu\rho\dfrac{X}{\sigma}-\dfrac{\mu(1+X)}{\sigma(1+\kappa)}}\frac{\kappa}{1+\kappa}+2\rho\left(1-\sigma^2\right)\frac{\left(\rho+\mu\dfrac{X}{\sigma}\right)\left((1+X)^2-\sigma^2\right)}{\rho^2+\mu\rho\dfrac{X}{\sigma}-\dfrac{\mu(1+X)}{\sigma(1+\kappa)}}\kappa\right]
\end{aligned}
\tag{A1}
$$

with

$$
\rho=\frac{\left(1-\sigma^2\right)\mu+(1+X)\left(\sigma+\dfrac{2\sigma\kappa}{1+\kappa}\right)}{\sigma(2+X)} \tag{A2}
$$

and

$$
\begin{aligned}
N_1 = &\,9-10\sigma^2+\sigma^4+\left(18-4\sigma^2-4\sigma^4\right)X+\left(15+3\sigma^2\right)X^2+\left(6+2\sigma^2\right)X^3+X^4\\
&+\kappa\left[21-10\sigma^2+\sigma^4+\left(42+2\sigma^2-4\sigma^4\right)X\right.\\
&\left.+\left(30+12\sigma^2\right)X^2+\left(9+5\sigma^2\right)X^3+X^4\right].
\end{aligned}
\tag{A3}
$$

The nonlinear coefficient N contains two terms proportional to κ, the second and last terms in the large brackets. For $\kappa \gg 1$ the last term goes to

$$
2\left(1-\sigma^2\right)\left((1+X)^2-\sigma^2\right)\kappa \tag{A4}
$$

https://doi.org/10.1017/jfm.2025.10214 Published online by Cambridge University Press

which cancels with the second term proportional to κ. When κ goes to infinity we obtain

$$N = -\frac{\omega k^2}{8\sigma^2}\left(\sigma^2\frac{5+3X}{2+X} - \frac{P_0+P_1X+P_2X^2+P_3X^3+X^4}{(3-\sigma^2+3X)(2+X)} + \frac{2((1+X)^2-\sigma^2)}{\rho_\infty} + \frac{2\left(1-\sigma^2\right)}{\rho_\infty+\mu X/\sigma}\right) \tag{A5}$$

with

$$\rho_\infty = \frac{\left(1-\sigma^2\right)\mu + 3\sigma(1+X)}{\sigma(2+X)} \tag{A6}$$

which is the limit of ρ when κ goes to infinity. Injecting the expression of ρ_∞ in (A5) gives (2.10).

References

Abid, M., Kharif, C., Hsu, H.-C. & Chen, Y.-Y. 2019 Transverse instability of gravity–capillary solitary waves on deep water in the presence of constant vorticity. *J. Fluid Mech.* **871**, 1028–1043.

Akylas, T.R. 1993 Envelope solitons with stationary crests. *Phys. Fluids A: Fluid Dyn.* **5** (4), 789–791.

Chen, B. & Saffman, P.G. 1985 Three-dimensional stability and bifurcation of capillary and gravity waves on deep water. *Stud. Appl. Maths* **72** (2), 125–147.

Constantin, A. & Kartashova, E. 2009 Effect of non-zero constant vorticity on the nonlinear resonances of capillary water waves. *Europhys. Lett.* **86** (2), 29001.

Crapper, G.D. 1957 An exact solution for progressive capillary waves of arbitrary amplitude. *J. Fluid Mech.* **2** (6), 532–540.

Dhar, A.K. & Kirby, J.T. 2023 Fourth-order stability analysis for capillary-gravity waves on finite-depth currents with constant vorticity. *Phys. Fluids* **35** (2), 026601.

Dias, F., Dyachenko, A.I. & Zakharov, V.E. 2008 Theory of weakly damped free-surface flows: a new formulation based on potential flow solutions. *Phys. Lett. A* **372** (8), 1297–1302.

Dias, F. & Kharif, C. 1999 Nonlinear gravity and capillary-gravity waves. *Annu. Rev. Fluid Mech.* **31** (1), 301–346.

Djordjevic, V.D. & Redekopp, L.G. 1977 On two-dimensional packets of capillary-gravity waves. *J. Fluid Mech.* **79** (4), 703–714.

Ellingsen, S.Å. 2014 Initial surface disturbance on a shear current: the Cauchy–Poisson problem with a twist. *Phys. Fluids* **26** (8), 082104.

Ellingsen, S.A. 2016 Oblique waves on a vertically sheared current are rotational. *Eur. J. Mech. B/Fluids* **56**, 156–160.

Hogan, S.J. 1985 The fourth-order evolution equation for deep-water gravity-capillary waves. *Proc. R. Soc. Lond. A. Math. Phys. Sci.* **402** (1823), 359–372.

Hogan, S.J. 1988 The superharmonic normal mode instabilities of nonlinear deep-water capillary waves. *J. Fluid Mech.* **190**, 165–177.

Hsu, H.C., Kharif, C., Abid, M. & Chen, Y.Y. 2018 A nonlinear schrödinger equation for gravity-capillary water waves on arbitrary depth with constant vorticity. part 1. *J. Fluid Mech.* **854**, 146–163.

Ifrim, M. & Tataru, D. 2020 No solitary waves in 2d gravity and capillary waves in deep water. *Nonlinearity* **33** (10), 5457–5476.

Kharif, C., Kraenkel, R.A., Manna, M.A. & Thomas, R. 2010 The modulational instability in deep water under the action of wind and dissipation. *J. Fluid Mech.* **664**, 138–149.

Kim, B. & Akylas, T.R. 2005 On gravity–capillary lumps. *J. Fluid Mech.* **540**, 337–351.

Longuet-Higgins, M.S. 1989 Capillary–gravity waves of solitary type on deep water. *J. Fluid Mech.* **200**, 451–470.

Longuet-Higgins, M.S. 1993 Capillary–gravity waves of solitary type and envelope solitons on deep water. *J. Fluid Mech.* **252**, 703–711.

Martin, C.I. 2017 Resonant interactions of capillary-gravity water waves. *J. Math. Fluid Mech.* **19** (4), 807–817.

Martin, C.I. & Matioc, B.-V. 2013 Existence of Wilton Ripples for water waves with constant vorticity and capillary effects. *SIAM J. Appl. Maths* **73** (4), 1582–1595.

https://doi.org/10.1017/jfm.2025.10214 Published online by Cambridge University Press

McLean, J.W. 1982*a* Instabilities of finite-amplitude gravity waves on water of finite depth. *J. Fluid Mech.* **114**, 331.

McLean, J.W. 1982*b* Instabilities of finite-amplitude water waves. *J. Fluid Mech.* **114**, 315.

Milewski, P.A. 2005 Three-dimensional localized solitary gravity-capillary waves. *Commun. Math. Sci.* **3** (1), 89–99.

Murashige, S. & Choi, W. 2021 Linear stability of transversely modulated finite-amplitude capillary waves on deep water. *Stud. Appl. Maths* **146** (2), 498–525.

Părău, E.I., Vanden-Broeck, J.-M. & Cooker, M.J. 2005 Nonlinear three-dimensional gravity–capillary solitary waves. *J. Fluid Mech.* **536**, 99–105.

Rypdal, K. & Rasmussen, J.J. 1989 Stability of solitary structures in the nonlinear schrödinger equation. *Phys. Scripta* **40** (2), 192–201.

Saffman, P.G. & Yuen, H.C. 1985 Three-dimensional waves on deep water. In *Advances in Nonlinear Waves* (ed. A. Jeffrey), vol. 2, pp. 1–10. Pitman.

Saffman, P.G. & Yuen, H.C. 1978 Stability of a plane soliton to infinitesimal two-dimensional perturbations. *Phys. Fluids* **21** (8), 1450–1451.

Segur, H., Henderson, D. & Carter, J. 2005 Stabilizing the Benjamin–Feir instability. *J. Fluid Mech.* **539**, 229–271.

Shats, M., Punzmann, H. & Xia, H. 2010 Capillary rogue waves. *Phys. Rev. Lett.* **104** (10), 104503.

Thomas, R., Kharif, C. & Manna, M. 2012 A nonlinear Schrödinger equation for water waves on finite depth with constant vorticity. *Phys. Fluids* **24** (12), 127102.

Tiron, R. & Choi, W. 2012 Linear stability of finite-amplitude capillary waves on water of infinite depth. *J. Fluid Mech.* **696**, 402–422.

Zakharov, V.E. & Rubenchik, A.M. 1974 Instability of waveguides and solitons in nonlinear media. *JETP* **38**, 494–500.

Zakharov, V.E. 1968 Stability of periodic waves of finite amplitude on the surface of a deep fluid. *J. Appl. Mech. Tech. Phys.* **9** (2), 190–194.

Zakharov, V.E. & Ostrovsky, L.A. 2009 Modulation instability: the beginning. *Physica D: Nonlinear Phenom.* **238** (5), 540–548.

Zhang, J. & Melville, W.K. 1986 On the stability of weakly-nonlinear gravity-capillary waves. *Wave Motion* **8** (5), 439–454.

https://doi.org/10.1017/jfm.2025.10214 Published online by Cambridge University Press